Dalton Transactions

PAPER

View Article Online
View Journal | View Issue

Cite this: *Dalton Trans.*, 2016, **45**, 681

Ligand noninnocence in FeNO corroles: insights from β-octabromocorrole complexes†

Hans-Kristian Norheim,[a] Jan Capar,[a] Rune F. Einrem,[a] Kevin J. Gagnon,[b] Christine M. Beavers,[b] Hugo Vazquez-Lima*[a] and Abhik Ghosh*[a]

Received 9th October 2015,
Accepted 29th October 2015

DOI: 10.1039/c5dt03947a

www.rsc.org/dalton

The first FeNO octabromocorroles have been synthesized including four β-octabromo-*meso*-tris(*p*-X-phenyl)corrole derivatives Fe[Br_8T*p*XPC](NO) (X = CF_3, H, CH_3, OCH_3) and the β-octabromo-*meso*-tris-(pentafluorophenyl)corrole complex, Fe[Br_8TPFPC](NO). The last complex, which proved amenable to single-crystal X-ray structure determination, exhibits the geometry parameters: Fe–N(O) 1.643(8) Å, N–O 1.158(9) Å, and a FeNO angle of 176.4(6)°. The more electron-deficient complexes exhibit increased instability with respect to NO loss and also higher infrared NO stretching frequencies (ν_{NO}). Interestingly, DFT calculations and IR marker bands indicate a noninnocent {FeNO}^{7}-(corrole$^{\bullet 2-}$) formulation for all FeNO corroles, both β-H_8 and β-Br_8, with essentially the same degree of corrole radical character. Instead, an electron-deficient corrole appears to exert a field effect resulting in reduced Fe-to-NO back-donation, which accounts for both the increased instability with respect to NO loss and the higher ν_{NO}'s.

Introduction

The well-known FeNO corroles have long been thought of as classic {FeNO}^{6} complexes.[1–3] Recently, multiple lines of evidence, including electronic absorption spectroscopy, infrared spectroscopy, and broken-symmetry DFT calculations,[4] however, have indicated a noninnocent {FeNO}^{7}-(corrole$^{\bullet 2-}$) formulation for these complexes.[5–9] The question thus arises, to what extent is such a description contingent upon the exact electronic character, *i.e.*, the substitution pattern, of the corrole? Our earlier study focused on FeNO complexes of *meso*-tris(*p*-X-phenyl)corrole ligands, *i.e.*, the Fe[T*p*XPC](NO) series. In this work, we have synthesized and characterized the corresponding β-octabromo complexes, *i.e.*, Fe[Br_8T*p*XPC](NO), where (Fig. 1; X = CF_3, H, CH_3, OCH_3), as well as Fe[Br_8TPFPC]-(NO), where Br_8TPFPC is the highly electron-deficient β-octabromo-*meso*-tris(pentafluorophenyl)corrole ligand. Qualitatively, the stability of the complexes appears to decrease as the corrole ligand becomes increasingly electron-deficient. Thus, it was gratifying that a single crystal X-ray structure could be obtained for Fe[Br_8TPFPC](NO), the most electron-deficient complex studied. Electron-poor FeNO corroles also exhibit higher infrared NO stretching frequencies (ν_{NO}), which vary over a range of some 40 cm^{-1}. It is tempting to interpret this trend as reflecting a slightly higher degree of {FeNO}^{6} character of the metal center, along with reduced radical character on the corrole. We shall see, however, that broken-symmetry DFT calculations indicate a different rationale.

Fig. 1 Fe[Br_8T*p*XPC](NO) derivatives studied in this work.

Results and discussion

Synthesis and chemical stability

The FeNO octabromocorroles were prepared in much the same manner as the corresponding β-H_8 complexes, *i.e.*, *via* iron

[a]*Department of Chemistry and Center for Theoretical and Computational Chemistry, UiT – The Arctic University of Norway, 9037 Tromsø, Norway.*
E-mail: hugo.vazquez@uit.no, abhik.ghosh@uit.no
[b]*Advanced Light Source, Lawrence Berkeley National Laboratory, One Cyclotron Road, Berkeley, CA 94720-8229, USA*

† Electronic supplementary information (ESI) available. CCDC 1430309. For ESI and crystallographic data in CIF or other electronic format see DOI: 10.1039/c5dt03947a

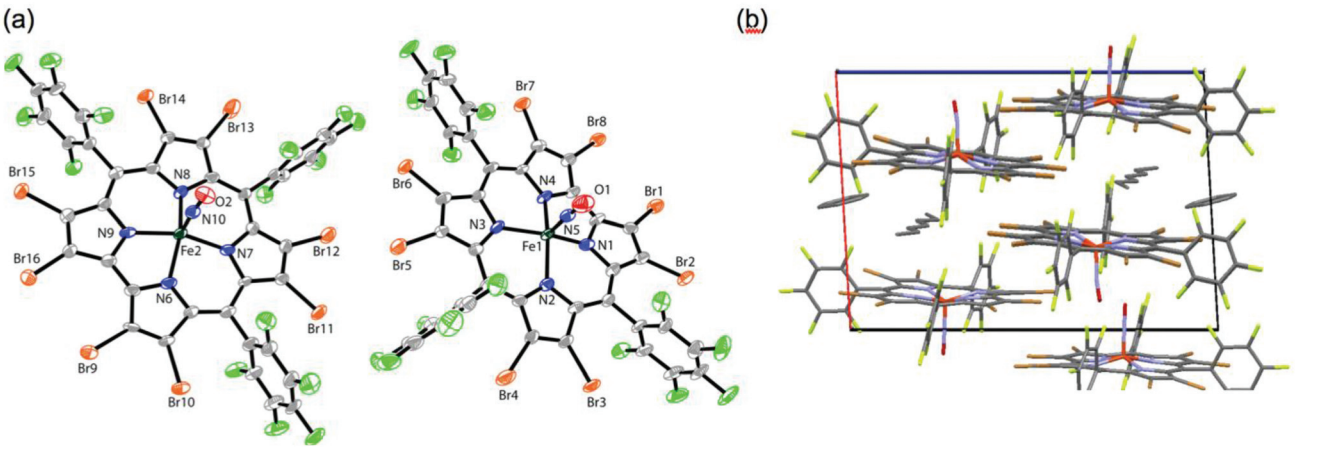

Fig. 2 X-ray structure of Fe[Br_8TPFPC](NO): (a) thermal ellipsoid plot and (b) stick representation of molecular packing. Selected distances (Å) and angles (°) involving the FeNO units: Fe1–N5 1.643(8), N5–O1 1.158(9), Fe1–N5–O1 176.4(6), Fe1–N1 1.900(7), Fe1–N2 1.952(7), Fe1–N3 1.931(7), Fe1–N4 1.928(6); Fe2–N10 1.655(7), N10–O2 1.143(9), Fe2–N10–O2 171.5(7), Fe2–N6 1.919(6), Fe2–N7 1.926(7), Fe2–N8 1.947(6), Fe2–N9 1.915(7).

insertion in pyridine-methanol, followed by addition of aqueous $NaNO_2$. The syntheses were greatly facilitated by the recent improvements in the syntheses of the H_3[Br_8T*p*XPC] (X = CF_3, H, CH_3, OCH_3)[10,11] and H_3[Br_8TPFPC] ligands.[12,13] The characteristic blood-red color of the FeNO complexes provided a simple visual test of their stability, which, as mentioned above, varied significantly across the compounds studied. Thus, Fe[T*p*XPC](NO), for X = H, CH_3, and OCH_3, and Fe[Br_8T*p*XPC](NO), for X = CH_3 and OCH_3, were all moderately stable in the solid state as well as overnight in dichloromethane solution at room temperature. On the other hand, blood-red dichloromethane and chloroform solutions of Fe[T*p*CF_3PC](NO), Fe[Br_8TPC](NO), Fe[TPFPC](NO), Fe[Br_8T*p*CF_3PC](NO), and Fe[Br_8TPFPC](NO), turned brown in about an hour or so, indicating decomposition. These complexes also decomposed, with NO loss, in the solid state, but only over days. Spectroscopic and electrochemical characterization was therefore carried out on freshly prepared samples, although certain measurements (particularly molar extinction coefficients and elemental analyses) could not be carried out for the more unstable complexes.

Molecular structure of Fe[Br_8TPFPC](NO) and general structural considerations[14]

Attempted crystallization and single-crystal X-ray analysis of Fe[Br_8T*p*CH_3PC](NO) led, to our surprise, to a rather poor-quality structure for a μ-oxodiiron 10-methoxyisocorrole complex. Fortunately, X-ray quality crystals of Fe[Br_8TPFPC]-(NO) could be obtained by diffusion of benzene into a heptane solution of the complex, providing the first X-ray structure of an FeNO octabromocorrole. The geometrical parameters of the FeNO units (listed under Fig. 2) were found to be nearly identical to those found for {FeNO}^{6} porphyrin-type complexes,[15] *i.e.*, Fe–N(O) ~1.65 Å, N–O ~1.16 Å, and a nearly linear FeNO angle >170°. We shall see, however, that other probes, notably infrared spectroscopy and broken-symmetry DFT calculations, favor a {FeNO}^{7}-(corrole$^{\bullet 2-}$) description, for both β-H_8 and β-Br_8 complexes.[16]

Despite the apparent similarity with {FeNO}^{6} complexes, careful examination of the skeletal bond distances of Fe-[Br_8TPFPC](NO) (Fig. 3), as well as those in DFT (B3LYP/STO-TZ2P) optimized structures, does afford evidence of corrole radical character. The bipyrrole part of the corrole macrocycle of Fe[Br_8TPFPC](NO) exhibits characteristic bond length alternations that are not seen in an innocent [Br_8TPFPC] complex such as Ir[Br_8TPFPC](Me_3N)$_2$.[17] Analogous bond length alternations have also been noted for noninnocent β-H_8 complexes such as Fe[TPC](NO) and Fe[TPC]Cl.[5] These bond length alternations all correspond to removal of an electron from the corrole HOMO depicted in Fig. 4.

Infrared spectroscopy

The infrared ν_{NO}'s of the FeNO octabromocorroles examined (1786–1803 cm^{-1}, Table 1) are some 90–100 cm^{-1} lower than those of genuine {FeNO}^{6} porphyrins such as Fe(TpivPP)(NO) (1893 cm^{-1}),[15] but some 30 cm^{-1} higher than the values measured for electron-rich FeNO corroles such as Fe[OEC]-(NO)[1] and Fe[TPC](NO)[4] (both 1767 cm^{-1}). Based on infrared ν_{NO}'s, the {FeNO}^{7}-(corrole$^{\bullet 2-}$) description proposed for β-H_8 FeNO triarylcorroles would appear to be applicable to the β-Br_8 complexes as well.

For β-H_8 FeNO corroles, the infrared ν_{NO}'s vary significantly as a function of the *meso* substituents, from 1761 cm^{-1} for Fe[T*p*OMePC](NO) to 1801 cm^{-1} for Fe[TPFPC](NO). Intriguingly, the effect of β-octabromination on the ν_{NO} varies considerably, from >20 cm^{-1} for certain Fe[Br_8T*p*XPC]-(NO) derivatives to only 2 cm^{-1} for Fe[Br_8TPFPC](NO), indicating a leveling-off with increasing electron-deficient character of the corrole ligand (Table 1). Indeed, a value of 1803 cm^{-1} appears to be the upper limit for the ν_{NO} of FeNO corroles.

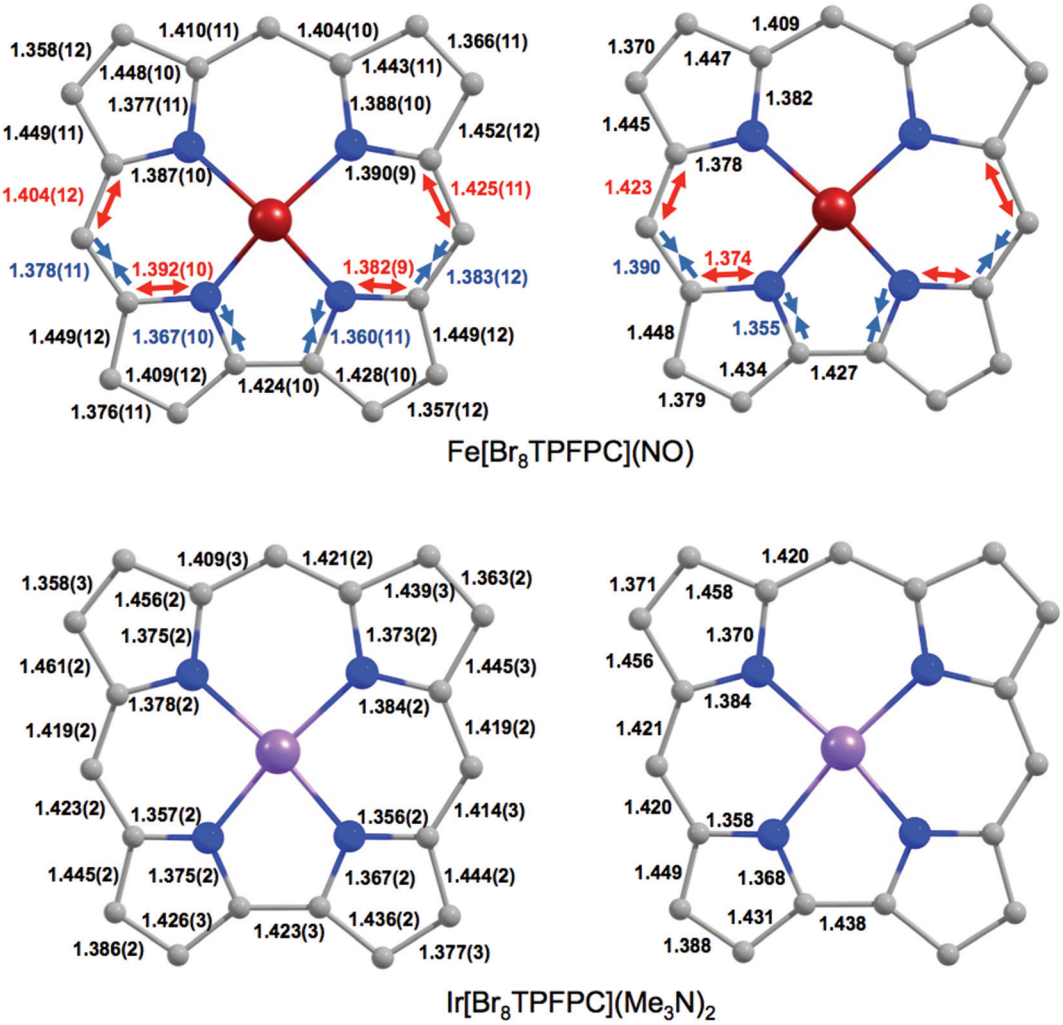

Fig. 3 Skeletal geometries (Å) of Fe[Br_8TPFPC](NO) and Ir[Br_8TPFPC]($Me_3N)_2$: X-ray (left) and B3LYP/STO-TZ2P (C_s, right) distances. The red and blue arrows indicate 'longer' and 'shorter' bonds, respectively.

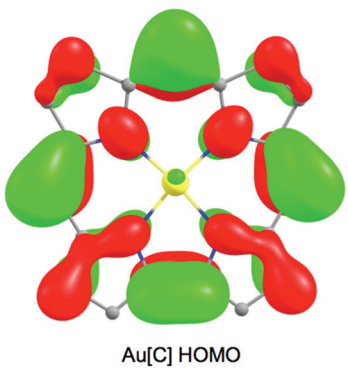

Fig. 4 The HOMO of Au(III) corrole, a representative innocent metallocorrole.

Table 1 Soret λ_{max} (nm), IR ν_{NO} (cm^{-1}), and redox potentials (V *vs.* SCE) of FeNO corroles

Complex	λ_{max}	ν_{NO}	$E_{1/2ox}$	$E_{1/2red}$
FeNO triarylcorroles				
Fe[T*p*OMePC](NO)	416	1761	0.83	−0.37
Fe[T*p*MePC](NO)	400	1767	0.84	−0.36
Fe[TPC](NO)	390	1767	0.86	−0.33
Fe[T*p*CO_2MePC](NO)	391	1770	0.95	−0.25
Fe[T*p*CF3PC](NO)	385	1781	0.98	−0.22
Fe[TPFPC](NO)	378	1801	1.07	0.00
FeNO β-octabromo-meso-triarylcorroles				
Fe[Br_8T*p*OMePC](NO)	394	1786	1.20	0.025
Fe[Br_8T*p*MePC](NO	395	1786	1.21	0.025
Fe[Br_8TPC](NO)	397	1794	—	—
Fe[Br_8T*p*CF_3PC](NO	391	1803	1.33	0.200
Fe[Br_8TPFPC](NO)	392	1803	—	—

'—': Data unavailable due to compound instability.

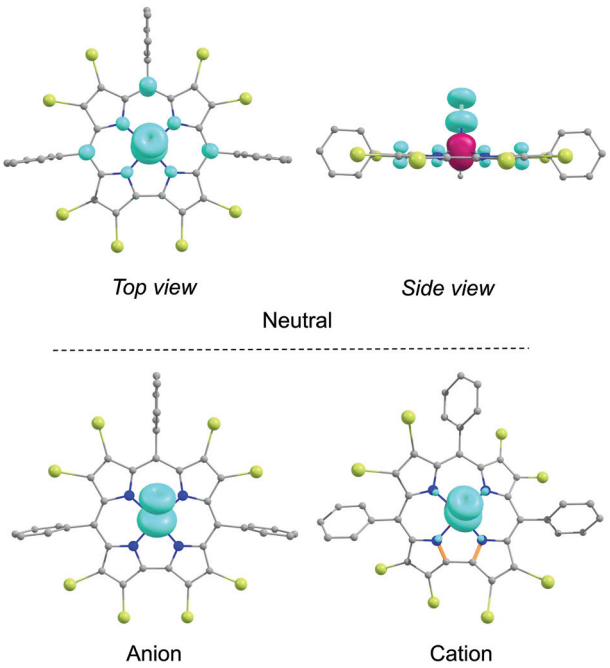

Fig. 5 Spin density plots for the neutral, anionic, and cationic states of Fe[Br_8TPC](NO). The α and β spin densities are shown in cyan and burgundy, respectively, The contour has been set at 0.009 e Å^{-3}.

Table 2 Selected broken-symmetry B3LYP/STO-TZP spin populations

Ligand	Fe	N	O	NO	Corrole
T*p*OMePC	2.031	−0.666	−0.488	−1.154	−0.877
TPC	2.018	−0.659	−0.486	−1.145	−0.873
TPFPC	1.949	−0.615	−0.477	−1.092	−0.857
Br_8T*p*OMePC	2.013	−0.627	−0.486	−1.113	−0.900
Br_8TPC	1.999	−0.620	−0.484	−1.104	−0.895
Br_8TPFC	1.918	−0.570	−0.467	−1.036	−0.882

DFT calculations

Broken-symmetry DFT (B3LYP) calculations played a major role in establishing the noninnocent, radical nature of FeNO corroles.[5] An examination of the broken-symmetry spin density profiles (Fig. 5) and Mulliken spin populations (Table 2) now also provide an attractive explanation for the variation of ν_{NO} across the complexes studied. Table 2 shows that both the Fe and NO spin populations decrease (in absolute value) with increasing electron-deficient character of the corrole ligand. Because the latter spin density may be viewed as a measure of occupation of the NO π* orbitals, we may conclude that a strongly electron-deficient corrole ligand leads to a lesser degree of backbonding and hence to a stronger NO bond and a higher ν_{NO}. Thus, between Fe[T*p*OMePC](NO) and Fe[Br_8TPFPC](NO), the magnitude of the broken-symmetry

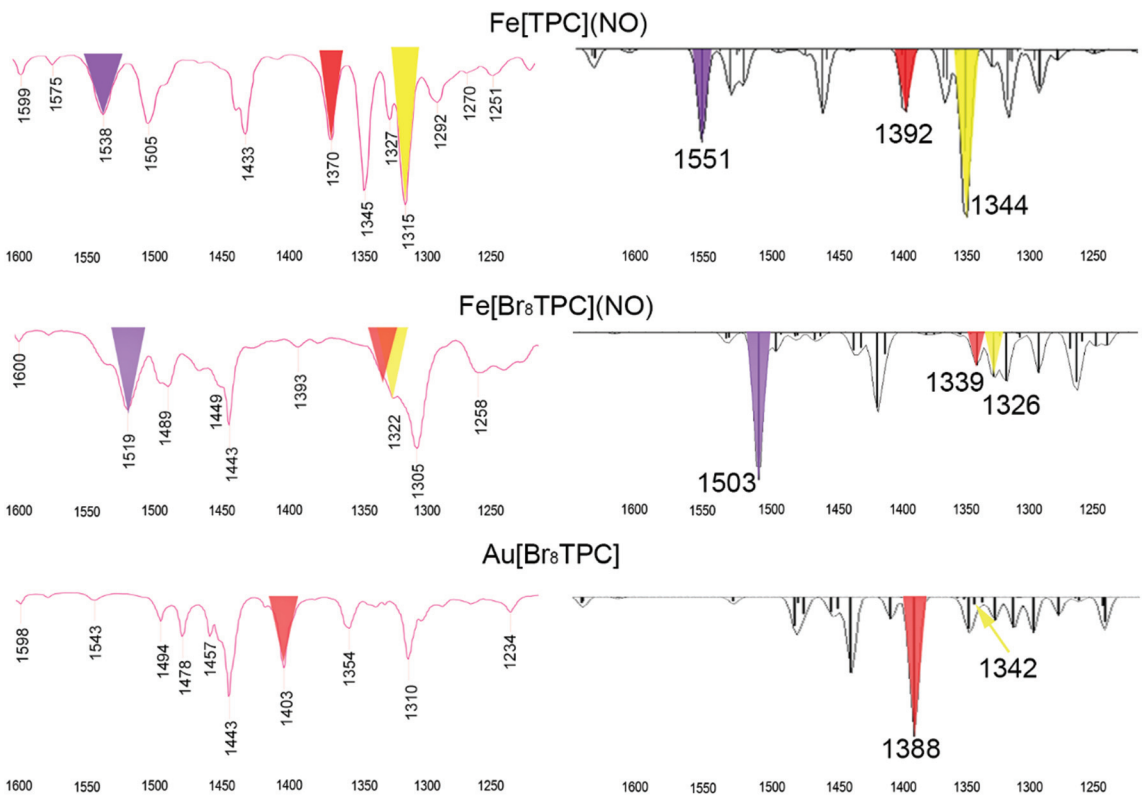

Fig. 6 Comparison of experimental and broken-symmetry B3LYP/STO-TZP calculated IR spectra for three metallocorroles.

spin population on the NO decreases by 0.12, which correlates with an experimentally observed upshift of 42 cm^{-1} in the ν_{NO}. Interestingly, there does not appear to be a clear correlation between the amount of broken-symmetry spin density on the macrocycle and its electron-deficient character. Indeed, to a first approximation, all FeNO corroles exhibit the same degree of corrole radical character (as measured by the amount of broken-symmetry spin density on the corrole).

In our earlier study of FeNO *meso*-triarylcorroles,[5] we identified 3–4 IR skeletal modes that are indicative of a noninnocent corrole macrocycle. Using IR spectroscopy and DFT calculations in concert, we have now identified the same modes for FeNO octabromocorroles (Fig. 6 and 7). Fig. 7 depicts the significant shifts in these bands between noninnocent Fe[Br_8TPC](NO) and the known, innocent analogue Au-[Br_8TPC]. These frequency shifts may be qualitatively interpreted in terms of changes in skeletal bond order as a result of removal of an electron from the corrole HOMO depicted in Fig. 4.

Redox potentials

As shown in Table 1, both the *meso* aryl and β-Br substituents exert a significant effect on the redox potentials of FeNO corroles. Thus, β-octabromination upshifts both the oxidation and reduction potentials by about 400 mV (Fig. 8). As shown in Fig. 5, the calculated spin densities of both the cationic and anionic states of a typical FeNO corrole are almost exclusively localized on the FeNO unit in a manner that is characteristic of a $S = 1/2$ $\{FeNO\}^7$ group. The corrole macrocycle in the cationic and anionic states thus may be described as formally monoanionic and trianionic, respectively, a scenario that is analogous to that observed for copper corroles.[18–21]

Electronic absorption spectroscopy

The Soret maxima of several but not all families of metallotriarylcorroles redshift markedly in response to increasing electron-donating character of the *para* substituent on the *meso*-aryl groups. Over a lengthy series of studies,[5,6,18,22–26] we have shown that this effect is specific to noninnocent corroles and the substituent effects arise from aryl-to-corrole charge transfer character in certain transitions in the Soret region. Indeed, the strongly substituent-sensitive Soret maxima of the Fe[T*p*XPC](NO) series provided the first clue that FeNO corroles are noninnocent, *i.e.* not $\{FeNO\}^6$.[5] The Fe[Br_8T*p*XPC]-(NO) series reported herein provides the first example of a series of noninnocent metallotriarylcorroles whose Soret

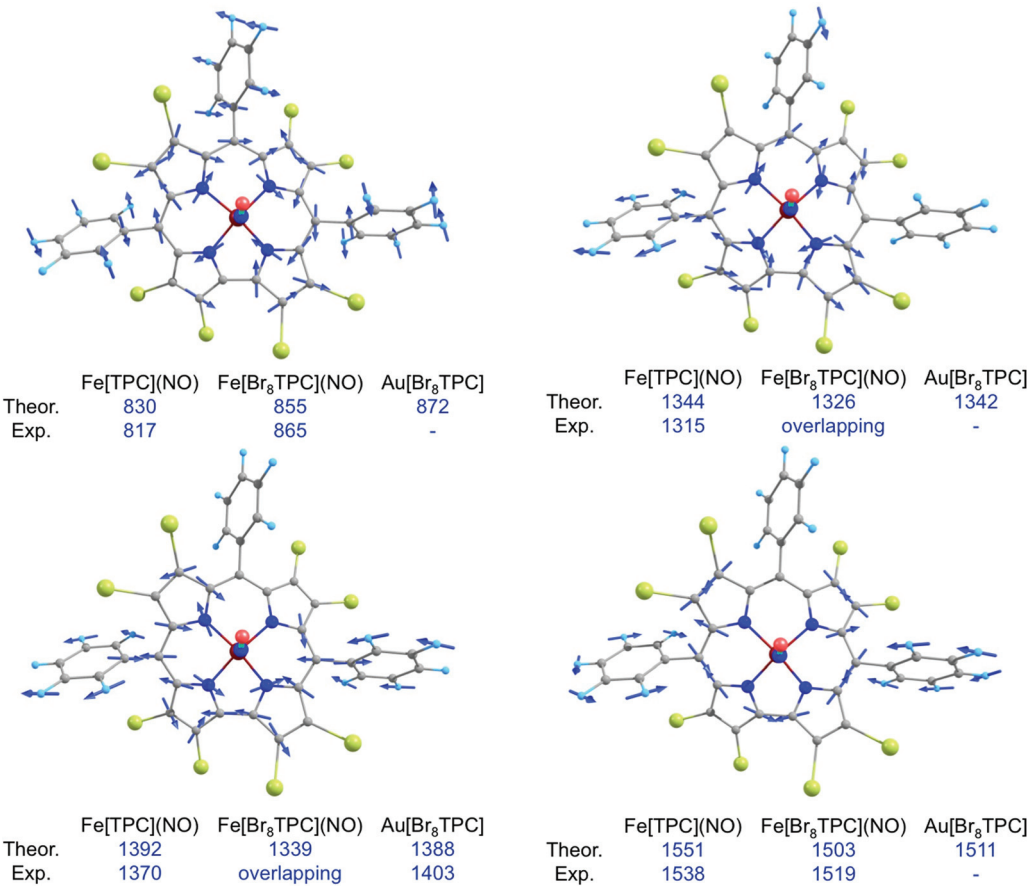

Fig. 7 Selected IR marker bands, including visual depiction of the eigenvectors and experimental and broken-symmetry B3LYP/STO-TZP frequencies (cm^{-1}).

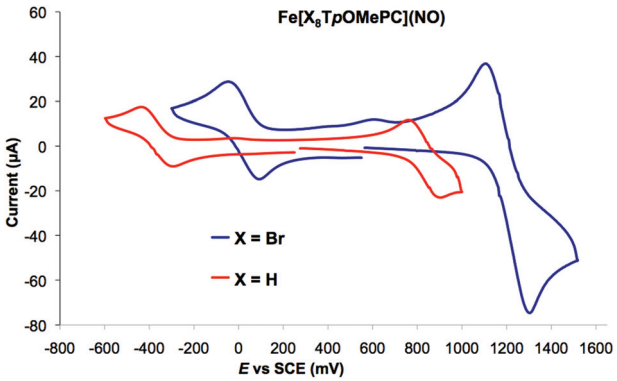

Fig. 8 Representative cyclic voltammograms of an FeNO triaarylcorrole and its β-Br_8 analogue.

maxima are essentially unaffected by *para* substituents on the *meso*-aryl groups (Table 1 and Fig. 9). Based on an examination of the valence MOs of the complexes in question, this unique behavior appears to be clearly attributable to steric inhibition of resonance, *i.e.*, the bulky β-Br groups preclude any significant mesomeric interactions between the aryl groups and the corrole macrocycle in these compounds. This scenario may be contrasted with the Cu[Br_8T*p*XPC] series, where strong saddling leads to enhanced aryl-corrole mesomeric interactions and hence also to strongly substituent-sensitive Soret maxima.[18a,d,e]

Conclusions

A detailed, multitechnique study of FeNO octabromocorroles has led to considerable deepening of our appreciation of FeNO corroles as strongly noninnocent complexes. Broken-symmetry DFT calculations indicate that the amount of radical character of the corrole macrocycle is essentially constant for all the FeNO corroles studied and does not vary significantly with increasing electron-deficient character of the corrole macrocycle. Instead, an electron-deficient corrole ligand leads to decreased π-backdonation from the iron to the NO, which manifests itself experimentally in a higher NO stretching frequency. The relative instability of the more electron-deficient FeNO corroles with respect to NO loss is also reasonably ascribed to decreased π-backdonation in these complexes.

A combined experimental-DFT approach has also led to the identification of structural and IR spectroscopic signatures for ligand noninnocence in FeNO corroles. Uniquely, the Soret maxima of FeNO octabromocorroles do not shift as a function of *para* substituents on the *meso*-aryl groups, as they do for other families of noninnocent metallotriarylcorroles. Steric inhibition of aryl-corrole mesomeric interactions in these sterically crowded complexes appears to be responsible for this unusual phenomenon.

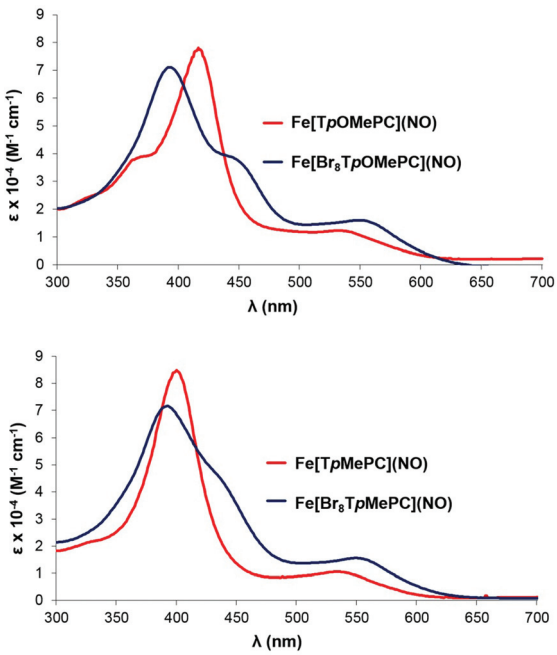

Fig. 9 Representative electronic absorption spectra.

Experimental section

Instrumentation

Ultraviolet–visible (UV–vis) spectra were recorded on an HP 8454 spectrophotometer in CH_2Cl_2. Cyclic voltammetry was carried out with an EG&G model 263A potentiostat equipped with a three-electrode system: a glassy carbon working electrode, a platinum wire counter electrode, and a saturated calomel reference electrode (SCE). Tetrabutylammonium perchlorate, recrystallized twice from absolute ethanol and dried in a desiccator for at least 2 weeks, was used as the supporting electrolyte. The reference electrode was separated from the bulk solution by a fritted-glass bridge filled with a solvent/supporting electrolyte mixture. All potentials were referenced to the SCE. A scan rate of 100 mV s^{-1} was used. The anhydrous CH_2Cl_2 solutions were purged with argon for at least 5 min prior to the electrochemical measurements and an argon blanket was maintained over the solutions during the measurements. ^{1}H NMR spectra (400 MHz) were recorded in $CDCl_3$ (referenced to residual $CHCl_3$ at 7.26 ppm) at 298 K on a Varian Inova 400 spectrometer. High-resolution electrospray-ionization (HR-ESI) mass spectra were recorded on an LTQ Orbitrap XL mass spectrometer. IR spectra were acquired as an average of 32 scans with a 1 cm^{-1} resolution on a Varian 7000e FT-IR spectrometer.

General synthetic details

All reagents and solvents were obtained from Sigma-Aldrich and used as purchased unless otherwise noted. CHROMASOLV® HPLC grade *n*-hexane and dichloromethane were used for chromatography. $FeCl_2{\cdot}4H_2O$ was obtained from Merck.

$NaNO_2$ was obtained from Fluka. Chloroform-*d* was obtained from Euriso-top. Pyrrole was passed through a short column of basic alumina (Merck, 5 cm height) before use to remove brownish impurities and stored at −20° C. Silica gel 60 (0.04–0.063 mm particle size; 230–400 mesh, Merck) was used for flash chromatography.

Free-base β-octabromo-*meso*-triarylcorroles $H_3[Br_8TpXPC]$[11] and $H_3[Br_8TPFPC]$[12] were prepared *via* the reductive demetalation of the copper and manganese complexes, respectively, as described earlier. For $H_3[Br_8TpXPC]$ (X = CH_3 and OCH_3), iron insertion and nitrosylation could be achieved in good yields *via* slight modification of a one-pot literature procedure.[2a] The procedure, however, did not work for $H_3[Br_8TPFPC]$ and led to relatively poor yields for $H_3[Br_8TPC]$ and $H_3[Br_8TpCF_3PC]$. In the latter two cases, the major byproduct could be readily converted to the FeCl corrole,[27] and subsequently nitrosylated *via* another literature procedure. For $H_3[Br_8TPFPC]$, a two-step procedure *via* Fe[TPFPC]Cl and subsequent nitrosylation was employed. All of the iron nitrosyl complexes were stored in sealed vials at 4 °C. Because of the limited stability of the compounds, especially with respect to denitrosylation, satisfactory elemental analyses did not prove possible. Full spectroscopic characterization was carried out on all the compounds and, in one case, also single-crystal X-ray structure determination. Detailed procedures for the preparation and purification of the various complexes are as follows.

Synthesis of Fe[$Br_8TpOMePC$](NO)

Free-base β-octabromo-*meso*-tris(4-methoxyphenyl)corrole (100 mg, 80 μmol) was added to a 50 mL two-necked round-bottomed flask equipped with a magnetic stirrer and a reflux condenser and dissolved in pyridine (4.0 mL) and methanol (8.0 mL). The system was the closed off with rubber septa and vented *via* an oil bubbler. Argon was bubbled through the solution while it was virgorously stirred for 20 min. Iron(II) chloride tetrahydrate (318 mg, 1.6 mmol) was added to the solution under an argon blanket. The solution was then heated to 69 °C under a slow flow of argon for 1 h after which heating was discontinued and a saturated aqueous solution of $NaNO_2$ (2.0 mL) was added dropwise *via* syringe, followed by stirring for an additional 30 min. The solution was then placed in an ice bath, quenched with cold water (40 mL), and filtered. The dry, filtered precipitate was washed with CH_2Cl_2 and the filtrate was rotary-evaporated to dryness. Flash chromatography (silica, 1 : 2 CH_2Cl_2 : hexane, subsequently 1 : 1) afforded Fe[Br_8TpOCH_3PC](NO) as the first, deep red band. Yield: 98 mg (92%). UV-vis (CH_2Cl_2): λ_{max} ($\varepsilon \times 10^{-4}$ (M^{-1} cm^{-1})) (nm); 394 (7.1), 549 (1.6). ^{1}H NMR (400 MHz, chloroform-*d*) δ 7.43 (br s, 4H, 5,15-*o*), 7.33 (d, J = 8.2 Hz, 2H, 10-*o*), 7.09 (d, J = 8.4 Hz, 4H, 5,15-*m*), 7.05 (d, J = 7.3 Hz, 2H, 10-*m*), 3.98 (s, 6H, 5,15-methoxy), 3.96 (s, 3H, 10-methoxy). MS (HR ESI) m/z 1330.4334 (M^-), calcd 1330.4340); IR (thin film): ν_{NO} 1786 cm^{-1}.

Synthesis of Fe[$Br_8TpMePC$](NO)

Free-base β-octabromo-*meso*-tris(4-methylphenyl)corrole (78 mg, 65 μmol) and iron(II) chloride tetrahydrate (259 mg, 1.3 mmol) were used as starting materials and subjected to the same procedure as described above. Flash chromatography (silica, 1 : 4 CH_2Cl_2/hexane) afforded Fe[Br_8TpCH_3PC](NO) as the first, deep red band. Yield: 76 mg (91%). UV-vis (CH_2Cl_2): λ_{max} ($\varepsilon \times 10^{-4}$ (M^{-1} cm^{-1})) (nm); 395 (7.2), 551 (1.6). ^{1}H NMR (400 MHz, chloroform-*d*) δ 7.47–7.29 (m, 5,10,15-aryl, 12H), 2.56 (s, 5,15-methyl, 6H), 2.55 (s, 10-methyl, 3H). MS (HR ESI) m/z 1283.4667 (M^-), calcd 1283.4556; IR (thin film): ν_{NO} 1786 cm^{-1}.

Synthesis of Fe[Br_8TPC](NO)

Free-base β-octabromo-*meso*-triphenylcorrole (42 mg, 36 μmol) and iron(II) chloride tetrahydrate (144 mg, 0.72 mmol) were subjected to the same procedure as described above. Flash chromatography (silica, 1 : 4 CH_2Cl_2 : hexane) afforded Fe[Br_8TPC](NO) as the first deep red band and also yielded second, darker reddish-brown band. The latter band was collected, evaporated to dryness, and dissolved in 20 mL CH_2Cl_2. The solution was washed twice with ~20 mL 7% $HCl_{(aq.)}$ and once with water, dried over $MgSO_4$, and filtered. A saturated aqueous solution of $NaNO_2$ (2.0 mL) was added to the solution, and the solution was stirred for 4 h at room temperature. The solution was washed with water, dried over $MgSO_4$, filtered, and evaporated to dryness. Flash chromatography (silica, 1 : 4 CH_2Cl_2 : hexane) afforded Fe[Br_8TPC](NO) as the first deep red band. Combined yield: 21 mg (47%). UV-vis (CH_2Cl_2): λ_{max} (ε relative) (nm); 397 (1.0), 553 (0.2). ^{1}H NMR (400 MHz, chloroform-*d*) δ 7.67–7.39 (m, 15H). MS (HR ESI) m/z 1240.3994 (M^-), calcd 1240.4013; IR (thin film): ν_{NO} 1794 cm^{-1}.

Synthesis of Fe[Br_8TpCF_3PC](NO)

Free-base β-octabromo-*meso*-tris(4-trifluoromethylphenyl)-corrole (127 mg, 93 μmol) and iron(II) chloride tetrahydrate (370 mg, 1.86 mmol) were subjected to the same procedure as described above, except that the reaction mixture was heated for 0.5 h instead of 1 h prior to $NaNO_2$ addition. Flash chromatography (silica, 1 : 4 CH_2Cl_2 : hexane) afforded Fe[Br_8TpCF_3PC](NO) as the first deep red band. Continued elution with 1 : 1 CH_2Cl_2 : hexane led to a second, reddish-brown band, which was collected and treated in the same way as described for the second band in the synthesis of Fe[Br_8TPC](NO) to yield a second crop of the title compound. Combined yield: 99 mg (74%). UV-vis (CH_2Cl_2): λ_{max} ($\varepsilon \times 10^{-4}$ (M^{-1} cm^{-1})) (nm); 392 (7.1), 552 (1.1). ^{1}H NMR (400 MHz, chloroform-*d*) δ 7.90–7.56 (m, 12H). MS (HR ESI) m/z 1444.3636 (M^-), (calcd 1444.3646); IR (thin film): ν_{NO} 1803 cm^{-1}.

Synthesis of Fe[Br_8TPFPC]Cl

Free-base β-octabromo-*meso*-tris(pentafluorophenyl)corrole (30 mg, 21 μmol) was added to a 50 mL two-necked round-

bottomed flask equipped with a magnetic stirrer and a reflux condenser and dissolved in dry DMF (25 mL). The system was the closed off with rubber septa and vented *via* an oil bubbler. Argon was bubbled through the solution under vigorous stirring for 20 min. Anhydrous iron(II) chloride (53 mg, 0.42 mmol) was added to the solution under an argon blanket and the solution was heated to reflux. The reaction was monitored by TLC (silica, CH_2Cl_2 : hexane 1 : 2). After 40 min of refluxing, no starting material could be detected by TLC and heating was discontinued. The solution was cooled to room temperature and the solvent removed *via* rotary evaporation. The solid material was dissolved in diethyl ether and passed through a short silica column with diethyl ether as eluent. After evaporation of the diethyl ether, the resulting solid was dissolved in CH_2Cl_2 and washed twice with 2 M $HCl_{(aq.)}$ and once with water. The organic layer was dried over Na_2SO_4 and evaporated to dryness. Flash chromatography (silica, CH_2Cl_2) afforded Fe[Br_8TPFPC]Cl as a reddish brown band. Yield: 29 mg (91%). UV-vis (CH_2Cl_2): λ_{max}, nm ($\log \varepsilon$, M^{-1} cm^{-1}) 418 (4.66), 563 (0.79).^{19}F NMR (376 MHz, chloroform-*d*) δ −151.05 (s, 2F), −151.83 (s, 4F), −157.73 (s, 3F), −159.60 (s, 6F). MS (MALDI-TOF) *m*/*z* 1480.69 ($M - Cl^-$), calcd 1480.47. MS (HR-ESI) *m*/*z* 1515.23 (M^-), calcd 1515.92.

Synthesis of Fe[Br_8TPFPC](NO)

Chloroiron β-octabromo-*meso*-tris(pentafluorophenyl)corrole (20 mg, 13 μmol) was dissolved in CH_2Cl_2 (20 mL) and a saturated aqueous solution of $NaNO_2$ (5.0 mL) was added to the solution. The solution was stirred at room temperature for 6 h, washed with water, dried over Na_2SO_4, and filtered, and the filtrate was evaporated to dryness. Flash chromatography (silica, 1 : 2 CH_2Cl_2 : hexane) of the residue afforded Fe[Br_8TPFPC](NO) as a deep red band. Yield: 13 mg (68%). X-ray quality crystals were obtained by vapor diffusion of *n*-heptane into a benzene solution of the title compound within a sealed vial. UV-vis (CH_2Cl_2): λ_{max}, nm ($\log \varepsilon$, M^{-1} cm^{-1}) 395 (5.52), 560 (1.28). ^{19}F NMR (376 MHz, Chloroform-*d*): δ −137.41 (dd, J = 23.7, 8.1 Hz, 5,15-*o*, 2F), −138.17 (d, J = 24.0 Hz, 10-*o*, 1F), −138.76 (d, J = 23.5 Hz, 10-*o*′, 1F), −138.99 (dd, J = 23.7, 7.9 Hz, 2F, 5,15-*o*′, 2F), −150.66 to −151.16 (m, 5,10,15-*p*, 3F), −161.57 to −162.41 (m, 5,10,15-*m*, 6F). MS (HR-ESI): 1510.26, (Calcd 1510.26). IR (thin film): ν_{NO} 1803 cm^{-1}.

Single-crystal X-ray structure determination of Fe[Br_8TPFPC](NO)·C_7H_{16}·0.5C_6H_6

A red block of 0.220 × 0.200 × 0.080 mm^3 was mounted in the 100(2) K nitrogen cold stream provided by an Oxford Cryostream low temperature apparatus on the goniometer head of a Bruker D85 diffractometer equipped with an ApexII CCD detector, on beamline 11.3.1 at the Advanced Light Source in Berkeley, CA. Diffraction data were collected using synchrotron radiation monochromated with silicon(111) to a wavelength of 0.77490(1) Å. A full sphere of data was collected using 0.3° ω scans. A multi-scan absorption correction was applied using the program SADABS 2014/3. The data consists of 54 540 reflections collected, of which 20 937 were unique [R(int) = 0.0627] and 13 555 were observed [$I > 2\sigma(I)$]. The structure was solved by dual-space methods (SHELXT) and refined by full-matrix least-squares on F^2 (SHELXL-97) using 1282 parameters and 0 restraints. The hydrogen atoms on carbon atoms were generated geometrically and refined as riding atoms with C–H = 0.95–0.99 Å and U_{iso}(H) = 1.2 times U_{eq}(C) for aromatic and CH_2 groups and U_{iso}(H) = 1.5 times U_{eq}(C) for CH_3 groups. The maximum and minimum peaks in the final difference Fourier map were 4.537 and −3.374 e $Å^{-3}$. Crystal data: $C_{84}H_{19}Br_{16}F_{30}Fe_2N_{10}O_2$, MW = 3160.35, triclinic, $P\bar{1}$, a = 13.667(3) Å, b = 16.679(3) Å, c = 20.152(4) Å, α = 74.769(3)°, β = 91.4200(10)°, γ = 88.903(3)°, V = 4425.1(15) $Å^3$, T = 100(2) K, Z = 2, R_1 [$I > 2\sigma(I)$] = 0.0702, wR_2 (all data) = 0.2084, GOF (on F^2) = 1.056.

Computational details

All calculations were carried out with the ADF 2014 [28] program system, the B3LYP[29,30] exchange–correlation functional, and appropriately fine integration grids and tight SCF and geometry optimization criteria. Scalar relativistic effects were taken into account with the ZORA Hamiltonian[31] and ZORA STO-TZP basis sets, except for the structures shown in Fig. 3, for which ZORA STO-TZ2P basis sets were employed.[32] Grimme's D3 dispersion correction was used throughout.[33] All optimized geometries were verified as true minima *via* numerical frequency calculations.

Acknowledgements

This work was supported by FRINATEK project 231086 of the Research Council of Norway (AG) and the Advanced Light Source, Berkeley, California (CMB, KJG). The Advanced Light Source is supported by the Director, Office of Science, Office of Basic Energy Sciences, of the U.S. Department of Energy under Contract No. DE-AC02-05CH11231

References

1 E. Vogel, S. Will, A. S. Tilling, L. Neumann, J. Lex, E. Bill, A. X. Trautwein and K. Wieghardt, *Angew. Chem., Int. Ed. Engl.*, 1994, **33**, 731–735.
2 (*a*) C. A. Joseph, M. S. Lee, A. V. Iretski, G. A. Wu and P. C. Ford, *Inorg. Chem.*, 2006, **45**, 2075–2082; (*b*) P. Singh, I. Saltsman, A. Mahammed, I. Goldberg, B. Tumanskii and Z. Gross, *J. Porphyrins Phthalocyanines*, 2012, **16**, 663–673; (*c*) W. Sinha, N. Deibel, H. Agarwala, A. Garai, D. Schweinfurth, C. S. Purohit, G. K. Lahiri, B. Sarkar and S. Kar, *Inorg. Chem.*, 2014, **53**, 1417–1429.
3 J. H. Enemark and R. D. Feltham, *Coord. Chem. Rev.*, 1974, **13**, 339–406.
4 Reviews on quantum chemical studies on nitrosyls: (*a*) A. Ghosh, *Acc. Chem. Res.*, 2005, **38**, 943–954; (*b*) A. Ghosh, K. H. Hopmann and J. Conradie, in *Computational Inorganic and Bioinorganic Chemistry*, ed. E. I. Solomon, R. A. Scott and R. B. King, John Wiley & Sons

Ltd, Chichester, UK, 2009, pp. 389–410; (*c*) L. E. Goodrich, F. Paulat, V. K. K. Praneeth and N. Lehnert, *Inorg. Chem.*, 2010, **49**, 6293–6316.

5 H. Vazquez-Lima, H.-K. Norheim, R. Einrem and A. Ghosh, *Dalton Trans.*, 2015, **44**, 10146–10151.

6 For earlier studies on ligand noninnocence in iron corroles from our aboratory, see: (*a*) E. Steene, T. Wondimagegn and A. Ghosh, *J. Phys. Chem. B*, 2001, **105**, 11406–11413; addition/correction: *J. Phys. Chem. B*, 2002, **106**, 5312–5312. (*b*) E. Steene, T. Wondimagegn and A. Ghosh, *J. Am. Chem. Soc.*, 2003, **125**, 16300–16309.

7 For other studies of ligand noninnocence in iron corroles, see: (*a*) O. Zakharieva, V. Schünemann, M. Gerdan, S. Licoccia, S. Cai, F. A. Walker and A. X. Trautwein, *J. Am. Chem. Soc.*, 2002, **124**, 6636–6648; (*b*) Review: F. A. Walker, S. Licoccia and R. Paolesse, *J. Inorg. Biochem.*, 2006, **100**, 810–837.

8 *Ab initio* CASSCF/CASPT2 studies on FeCl corrole: B. O. Roos, V. Veryazov, J. Conradie, P. R. Taylor and A. Ghosh, *J. Phys. Chem.*, 2008, **112**, 14099–14102.

9 A. B. Alemayehu, H. Vazquez-Lima, C. M. Beavers, K. J. Gagnon, J. Bendix and A. Ghosh, *Chem. Commun.*, 2014, **50**, 11093–11096.

10 C. Capar, K. E. Thomas and A. Ghosh, *J. Porphyrins Phthalocyanines*, 2008, **12**, 964–967.

11 J. Capar, S. Berg, K. E. Thomas, C. M. Beavers, K. J. Gagnon and A. Ghosh, *J. Inorg. Biochem.*, in press: http://www.sciencedirect.com/science/article/pii/S0162013415300441.

12 C. Capar, L.-K. Hansen, J. Conradie and A. Ghosh, *J. Porphyrins Phthalocyanines*, 2010, **14**, 509–512.

13 For a crystal structure of $H_3[Br_8TPFPC]$, see: J. Capar, J. Conradie, C. M. Beavers and A. Ghosh, *J. Phys. Chem. A*, 2015, **119**, 3452–3457.

14 For reviews on corrole coordination chemistry, see: (*a*) K. E. Thomas, A. Alemayehu, J. Conradie, C. M. Beavers and A. Ghosh, *Acc. Chem. Res.*, 2012, **45**, 1203–1214; (*b*) J. H. Palmer, *Struct. Bonding*, 2012, **142**, 49–89; (*c*) H. L. Buckley and J. Arnold, *Dalton Trans.*, 2015, **44**, 30–36.

15 M. K. Ellison, C. E. Schulz and W. R. Scheidt, *Inorg. Chem.*, 1999, **38**, 100–108.

16 For key examples of linear, $S = 1/2$ $\{FeNO\}^7$ complexes, see: (*a*) K. J. Franz and S. J. Lippard, *J. Am. Chem. Soc.*, 1999, **121**, 10504–10512; addition/correction: *J. Am. Chem. Soc.*, 2001, **123**, 1266–1266; (*b*) For a theoretical study, see: E. Tangen, J. Conradie and A. Ghosh, *Inorg. Chem.*, 2005, **44**, 8699–8706; (*c*) J. Conradie, K. H. Hopman and A. Ghosh, *J. Phys. Chem. B*, 2010, **114**, 8517–8524.

17 J. H. Palmer, M. W. Day, A. D. Wilson, L. M. Henling, Z. Gross and H. B. Gray, *J. Am. Chem. Soc.*, 2008, **130**, 7786–7787.

18 For selected studies of Cu corroles from our laboratory, see: (*a*) I. H. Wasbotten, T. Wondimagegn and A. Ghosh, *J. Am. Chem. Soc.*, 2002, **124**, 8104–8116; (*b*) A. B. Alemayehu, E. Gonzalez, L.-K. Hansen and A. Ghosh, *Inorg. Chem.*, 2009, **48**, 7794–7799; (*c*) A. B. Alemayehu, L.-K. Hansen and A. Ghosh, *Inorg. Chem.*, 2010, **49**, 7608–7610; (*d*) K. E. Thomas, J. Conradie, L.-K. Hansen and A. Ghosh, *Eur. J. Inorg. Chem.*, 2011, 1865–1870; (*e*) S. Berg, K. E. Thomas, C. M. Beavers and A. Ghosh, *Inorg. Chem.*, 2012, **51**, 9911–9916.

19 For key early papers on Cu corroles, see: (*a*) C. Brückner, R. P. Briñas and J. A. K. Bauer, *Inorg. Chem.*, 2003, **42**, 4495–4497; (*b*) M. Bröring, F. Brégier, E. C. Tejero, C. Hell and M. C. Holthausen, *Angew. Chem., Int. Ed.*, 2007, **46**, 445–448.

20 For spectroelectrochemical studies of Cu corroles, see: Z. Ou, J. Shao, H. Zhao, K. Ohkubo, I. H. Wasbotten, S. Fukuzumi, A. Ghosh and K. M. Kadish, *J. Porphyrins Phthalocyanines*, 2004, **8**, 1236–1247.

21 The $Fe[Br_8TpXPC](NO)$ complexes appear to exhibit a two-electron oxidation; the origin of this phenomenon remains to be investigated.

22 MnCl corroles: A. Ghosh and E. Steene, *J. Inorg. Biochem.*, 2002, **91**, 423–436.

23 CrO and MoO corroles: I. Johansen, H.-K. Norheim, S. Larsen, A. B. Alemayehu, J. Conradie and A. Ghosh, *J. Porphyrins Phthalocyanines*, 2011, **15**, 1335–1344.

24 TDDFT studies of Cu corroles: (*a*) A. B. Alemayehu, J. Conradie and A. Ghosh, *Eur. J. Inorg. Chem.*, 2011, **12**, 1857–1864; (*b*) A. B. Alemayehu, M. M. Conradie and A. Ghosh, *J. Porphyrins Phthalocyanines*, 2012, **16**, 695–704.

25 Ag and Au corroles: (*a*) Au: A. B. Alemayehu and A. Ghosh, *J. Porphyrins Phthalocyanines*, 2011, **15**, 106–110; (*b*) Ag, Au: K. E. Thomas, A. B. Alemayehu, J. B. Conradie, C. M. Beavers and A. Ghosh, *Inorg. Chem.*, 2011, **50**, 12844–12851. Ag, Au: K. E. Thomas, H. Vazquez-Lima, Y. Fang, Y. Song, K. J. Gagnon, C. M. Beavers, K. M. Kadish and A. Ghosh, *Chem. – Eur. J.*, 2015, **21**, 16839–16847.

26 5d metallocorroles: (*a*) Pt: A. B. Alemayehu, H. Vazquez-Lima, C. M. Beavers, K. J. Gagnon, J. Bendix and A. Ghosh, *Chem. Commun.*, 2014, **50**, 11093–11096; (*b*) Os: A. Alemayehu, K. J. Gagnon, J. Terner and A. Ghosh, *Angew. Chem., Int. Ed.*, 2014, **53**, 14411–14414.

27 L. Simkhovich, A. Mahammed, I. Goldberg and Z. Gross, *Chem. – Eur. J.*, 2001, **7**, 1041–1055.

28 (*a*) G. te Velde, F. M. Bickelhaupt, S. J. A. van Gisbergen, C. Fonseca Guerra, E. J. Baerends, J. G. Snijders and T. Ziegler, *J. Comput. Chem.*, 2001, **22**, 931–967; (*b*) C. Fonseca Guerra, J. G. Snijders, G. te Velde and E. J. Baerends, *Theor. Chem. Acc.*, 1998, **99**, 391–403.

29 A. D. Becke, *Phys. Rev.*, 1988, **A38**, 3098–3100.

30 C. Lee, W. Yang and R. G. Parr, *Phys. Rev. B: Condens. Matter*, 1998, **37**, 785–789.

31 (*a*) E. van Lenthe, E. J. Baerends and J. G. Snijders, *J. Chem. Phys.*, 1993, **99**, 4597–4610; (*b*) E. van Lenthe, E. J. Baerends and J. G. Snijders, *J. Chem. Phys.*, 1994, **101**, 9783–9792; (*c*) E. van Lenthe, A. E. Ehlers and E. J. Baerends, *J. Chem. Phys.*, 1999, **110**, 8943–8953.

32 E. van Lenthe and E. J. Baerends, *J. Comput. Chem.*, 2003, **24**, 1142–1156.

33 S. Grimme, J. Antony, S. Ehrlich and H. Krieg, *J. Chem. Phys.*, 2010, **132**, 154104.